

Supporting Information

A Versatile Platform of Poly(acrylic acid) Cryogel for Highly Efficient Photothermal Water Evaporation

Jia-Yun Wang^a, Xiao-Xiao Guo^a, Jun Chen^a, Hou-Shi Chang^a, Hui-Juan Li^a, Abdul Haleem^a, Sheng-Qi Chen^b, Wei-Dong He^{*a}

^a:CAS Key Laboratory of Soft Matter Chemistry, Department of Polymer Science and Engineering, University of Science and Technology of China, Hefei, Anhui 230026, China
^b: Key Laboratory of Xin'an Medicine, Ministry of Education; Engineering Technology Research Center of Modernized Pharmaceuticals, Anhui Province; Anhui University of Chinese Medicine, Hefei, Anhui 230038, China.

Preparation of graphene oxide (GO)

GO was prepared according to Hummers' method^{1, 2}. After graphite powder and sodium nitrite were added into a round-bottom flask kept in an ice bath, 98% H₂SO₄ was carefully added dropwise under magnetic stirring, followed by the addition of KMnO₄ powder in 15 min. The mixture stood at 3 °C for 40 min and diluted with distilled water at room temperature. Then, in an oil bath, the mixture was stirred vigorously at 98 °C for an additional 15 min. At room temperature, the mixture was transferred into a flask and charged with distilled water and H₂O₂. After being stirred for 2 min, the sediment was obtained by centrifugation and re-dispersed into hot water at 60 °C. Then, HCl aqueous solution (12 mol/L) was added dropwise. After stirring for 5 min, the final product of GO was obtained by centrifugation, twice washing with a large amount of distilled water and freezing-dryness.

Assembly of crygel sheet and mushroom-shaped crygel into evaporation system

The mould is made up of one 1.5 mL centrifugal tube with a height of 30 mm and one discoid container (diameter = 50 mm, height = 5 mm) as shown in Figure S1a. Both one composite crygel sheet and the top of one mushroom-shaped crygel was cut into the disk shape with 30 mm diameter. Then, they were assembled inside PSt foam with the sheet attached to the top of mushroom-shaped crygel (Figure S1b). The diameter and thickness of one PAAc crygel sheet are shown in Figure S1c and S1d.

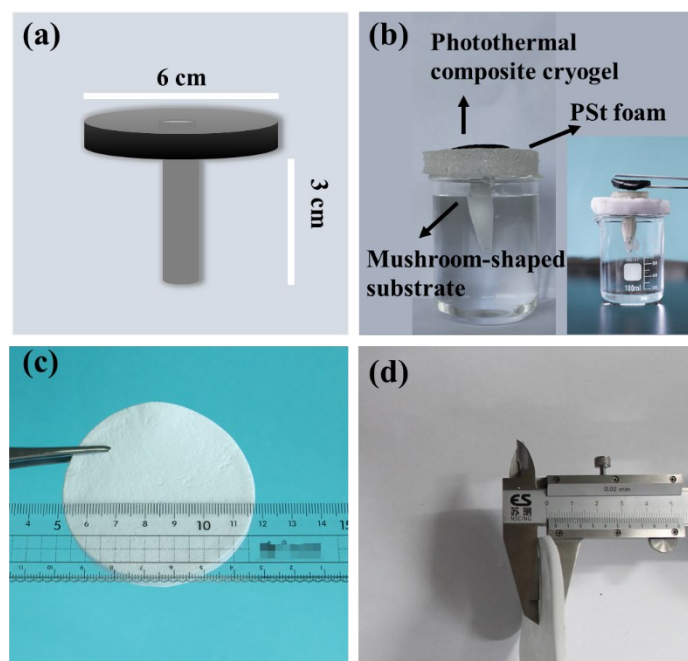


Figure S1 (a) The mould for synthesizing mushroom-shaped PAAc crygel as the substrate, (b) the photothermal evaporation system with water reservoir (The inset shows that the photothermal layer and the substrate can be separated), (c) diameter record of one crygel sheet and (d) thickness record of one crygel sheet.

For PPy and PANI, the in-situ polymerization of pyrrole and aniline inside pure PAAc cryogel resulted in PAAc-PPy and PAAc-PANI cryogel, respectively. For GO, the cryopolymerization of acrylic acid in the presence of GO produced PAAc-GO cryogel, which was converted into PAAc-rGO cryogel by the reduction with ascorbic acid. Afterwards, with the aid of PSt foam, one cryogel sheet and one mushroom-shaped cryogel, as two modules, were assembled into the photothermal evaporation system, as illustrated in Scheme 1. The appearance of different cryogels are shown in Figure S1 and Figure S2. After the incorporation of photothermal materials, white PAAc composite cryogel turns coloured. Additionally, after the reduction of GO with ascorbic acid, PAAc-rGO cryogel becomes black from the brown colour of PPy-GO cryogel.

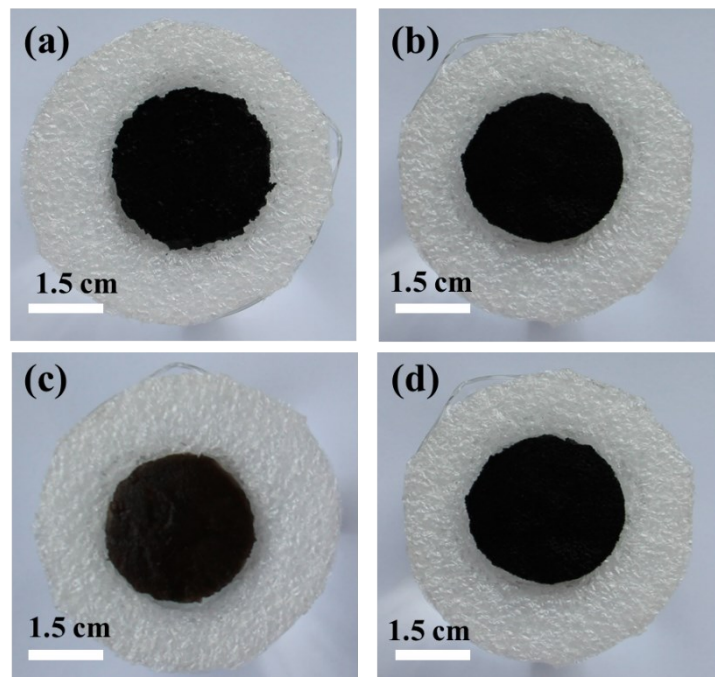
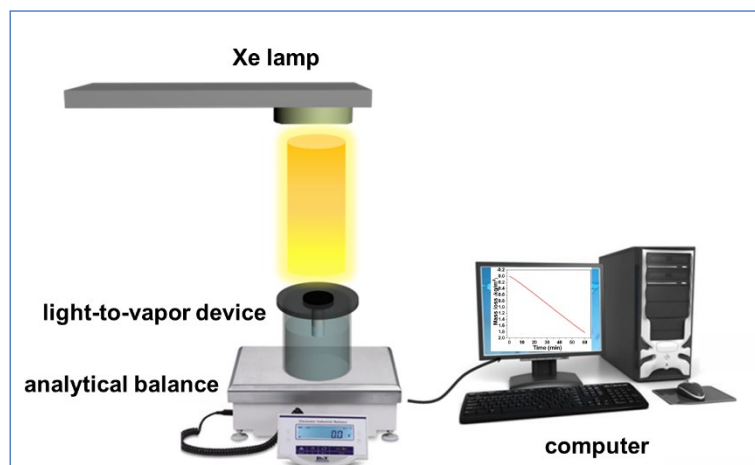


Figure S2 Digital photographs of PAAc-PPy (a), PAAc-PANI (b), PAAc-GO (c) and PAAc-rGO (d) cryogel sheet embedded in PSt foam.

Photothermal evaporation measurement was performed with one self-made setup as shown in Scheme S1.



Scheme S1 Schematic setup for photothermal evaporation measurement.

Determination of gel fraction of cryogel and hydrogel

To estimate the monomer conversion, the produced cryogel/hydrogel was kept in distilled water (200 mL) at room temperature for 12 h and lyophilized to constant weight. Based on the weight of left cryogel/hydrogel, monomer conversion was determined. Afterwards, the dried and weighed cryogel/hydrogel was soaked in deionized water for at least 48 h with exchanging distilled water every 4 h. Then, the swollen cryogel/hydrogel was lyophilized to constant weight. Based on the weights ratio before and after swelling, gel fraction of hydrogel was found to be more than 93% and that of cryogel above 95%.

FTIR and Raman analysis of cryogel and hydrogel

TIR spectra of different cryogels are demonstrated in Figure S3a. The characteristic absorbance signals of PAAc component are clearly observed, such as C=O stretching vibration (1715 cm^{-1}) and C-O stretching vibration (1252 cm^{-1}). The absorbance bands at 1456 and 1406 cm^{-1} are attributed to the in-plane deformation vibration of the C-O-H band^{3,4}. In the cases of PAAc-PPy and PAAc-PANI cryogels, this main signal of C=O have a red shifts to 1696 cm^{-1} and 1698 cm^{-1} because of the interaction of Py and ANI with carbonyl groups of PAAc. For the spectrum of PAAc-PPy cryogel, a weak signal at 1541 cm^{-1} is due to the C=C stretching vibration of Py ring^{5,6}. There is a weak signal at 1290 cm^{-1} being attributed to C-N stretching vibration while the bands at 785 and 920 cm^{-1} verify the presence of polymerized pyrrole. As for PAAc-PANI cryogel, a signal at 1610 cm^{-1} is attributed to the absorbance of benzoquinone structure. The signal at 1458 cm^{-1} belongs to stretching vibration of N=Q=N (Q=quinoid)⁷, which are in accordance with literature⁸. All of these characteristic signals prove that pyrrole and aniline have introduced into PAAc cryogel.

Raman spectra of PAAc-GO and PAAc-rGO cryogels in Figure S3b indicate the presence of D-band (1351 cm^{-1}) to G-band (1600 cm^{-1}), being characteristic of graphene. The intensity ratio of D-band to G-band (I_D/I_G) increases from 0.96 (PAAc-GO) to 1.24 (PAAc-rGO), suggesting the occurrence of reduced process⁹.

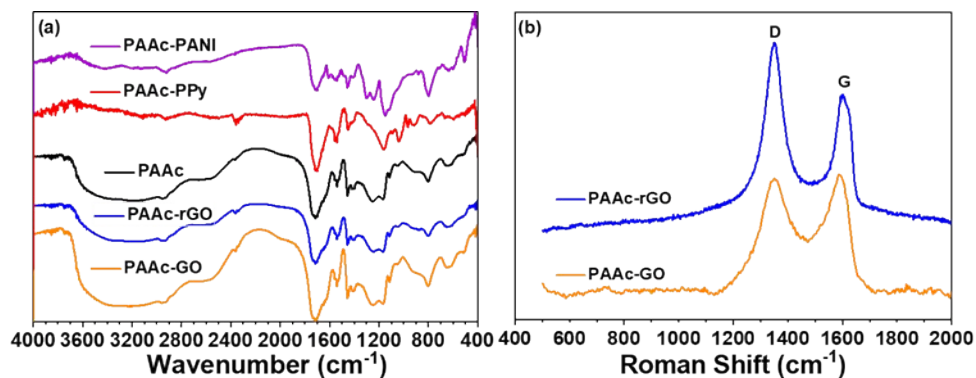


Figure S3 (a) FTIR spectra of different cryogels and (b) Raman spectra of PAAc-GO and PAAc-rGO cryogels.

TGA analysis of different cryogels

TGA thermograms of different cryogels are shown in Figure S4a and the variations of derivative weight with temperature are given in Figure S4b.

In the first stage of (below $100\text{ }^{\circ}\text{C}$), all materials show different weight losses due to the loss of physically absorbed water. For pure PAAc cryogel, the second stage of weight loss occurs between 165 and $306\text{ }^{\circ}\text{C}$ with 21% mass loss mainly due to the formation of anhydride. The third stage with 56% weight loss in the range of $306 \sim 505\text{ }^{\circ}\text{C}$ is caused by the carbonization of PAAc component. When the temperature reaches $800\text{ }^{\circ}\text{C}$, PAAc cryogel retains 7% weight retention. The thermal degradation behaviour of both PAAc-GO and PAAc-rGO cryogel is quite similar to that of PAAc cryogel but the final left mass is a little higher, due to the higher thermal stability of graphene. However, the thermal degradation behaviour of PAAc-PPy cryogel is obviously different. The weight loss is much slow as shown in Figure S4a as well as the derivative weight curve (Figure S4b). Up to $800\text{ }^{\circ}\text{C}$, PAAc-PPy cryogel still has 20% weight retention. PAAc-PANI cryogel also exhibits retarded weight loss at high temperatures above $450\text{ }^{\circ}\text{C}$. The acid-doping ability, i.e. the strong interaction of PAAc with PPy and PANI, is assumed to be the promising reason to enhance the thermal stability of those two composite cryogels.

PAAc-PPy and PAAc-PANI cryogels exhibit different degradation behaviour, suggesting that the strong interaction between PAAc and two photothermal polymers affect the dehydration and de-carboxylation of PAAc.

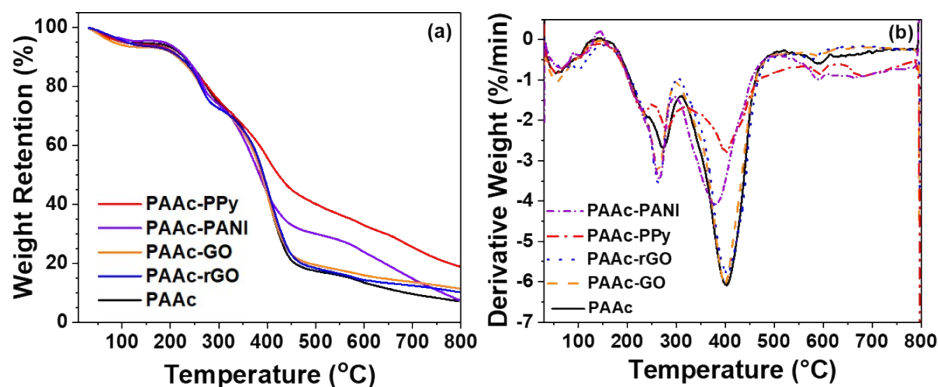


Figure S4 TGA thermograms (a) and their derivative weight loss (b) of different cryogels

Determination of porosity of cryogels and PAAc hydrogel

The porosity (ϕ , vol%) was determined based on the apparent density of cryogel/hydrogel and the real density of different components. The real density of composite cryogel is calculated based on the weight fraction of PAAc and photothermal material, where those for GO and rGO is taken as graphene density. The data are summarized in Table S1.

Table S1 The density and porosity of all the materials

sample	apparent density (ρ , g/cm ³)	real density (ρ_0 , g/cm ³)	porosity (ϕ , vol%)
PAAc cryogel	0.1357	1.2000	89 %
PAAc-PPy cryogel	0.1450	1.1767	88 %
PAAc-PANI cryogel	0.1708	1.1827	86 %
PAAc-GO cryogel	0.1506	1.2106	88 %
PAAc-rGO cryogel	0.1623	1.2063	87 %
PAAc hydrogel	0.3598	1.2000	70 %

Determination of porosity and pore area with mercury porosimeter

PAAc cryogel and hydrogel were studied with mercury porosimeter as shown in Figure S5. Based on the pore size distribution, PAAc cryogel has higher porosity and pore area with average pore size of 28 μm .

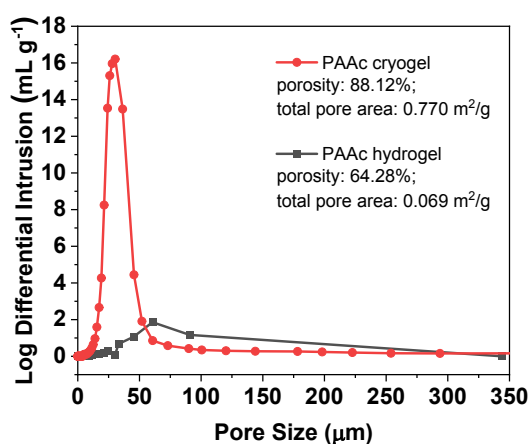


Figure S5 Channel size distribution, porosity and total channel area of pure PAAc cryogel and hydrogel.

Element mapping of PAAc-PPy and PAAc-PANI cryogels with STEM-EDX

PAAc-PPy and PAAc-PANI cryogels contain nitrogen element. As shown in Figure S5 and S6, the pattern of N mapping image is quite similar to those of C and O mapping images, confirming the uniform distribution of PPy and PANI inside PAAc cryogels.

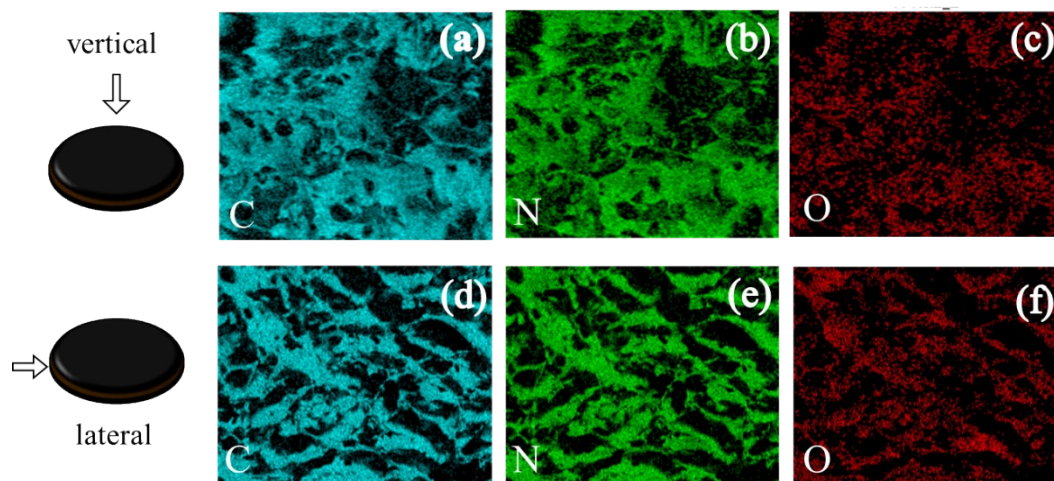


Figure S6 Vertical (a-c) and lateral (d-f) viewing element mapping images of C (a and d), N (b and e) and O (c and f) elements in PAAc-PPy cryogel.

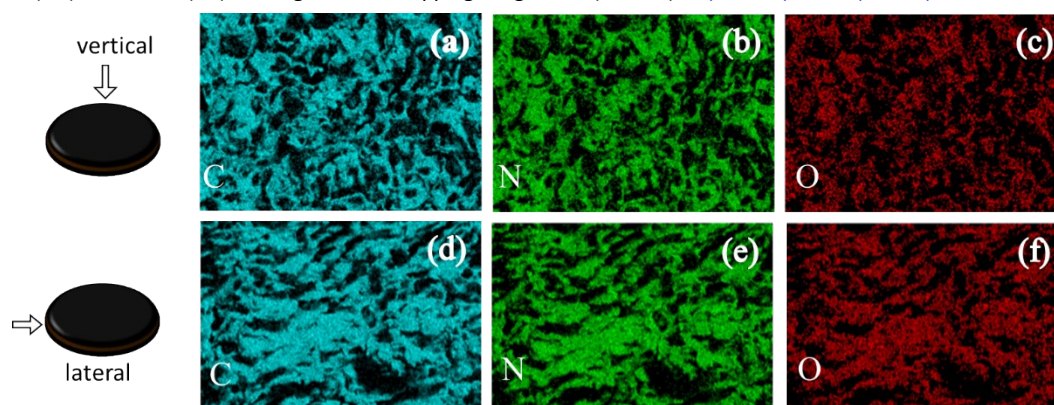


Figure S7 Vertical (a-c) and lateral (d-f) viewing element mapping images of C (a and d), N (b and e) and O (c and f) elements in PAAc-PANI cryogel.

Survey for wavenumber shift of FTIR absorbance for cryogels

To clarify the interaction between PAAc and different photothermal materials, the wavenumber shift of characteristic signals are surveyed and the local FTIR spectra are shown in Figure S7.

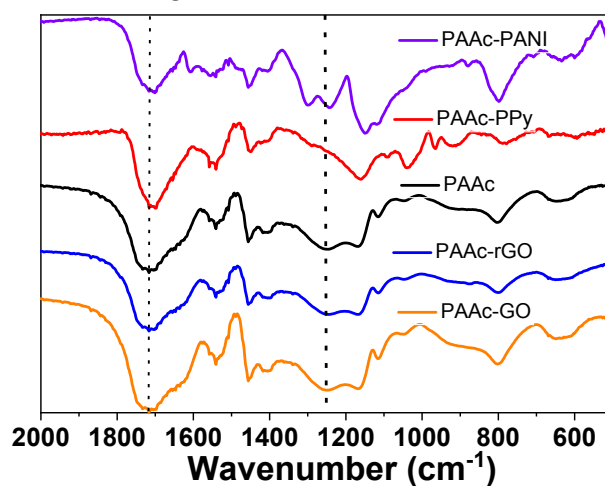


Figure S8 The local scan of FTIR spectra of different cryogels.

Temperature of cryogel sheet under one-sun irradiation for 60 min and the related light absorption efficiency

The surface temperature of cryogel sheet with mushroom-shaped PAAc cryogel substrate was recorded under one-sun irradiation for 60 min. The average and maximum temperatures for different cryogels are summarized in Table S2. The temperature difference between cryogel sheet and water reservoir was taken as average temperature (T_{ave}) minus room temperature (25 °C).

Table S2 Overall light absorption efficiency, average and maximum surface temperatures of different cryogel sheet under one-sun irradiation during photothermal evaporation of pure water.

Cryogel	η_{abs} (%)	T_{ave} (°C)	T_{max} (°C)	ΔT (°C)
PAAc	12.41	34.0	35.0	9.0
PAAc-PPy	97.49	41.3	44.1	16.3
PAAc-PANI	96.28	41.7	44.1	16.7
PAAc-GO	66.94	41.5	43.2	16.5
PAAc-rGO	85.47	40.8	43.7	15.8

IR camera images of dry cryogels under one-sun irradiation for 20 min

The surface temperature of different dry cryogel sheet was recorded as shown in Figure S9 with the maximum temperature annotated in each photo.

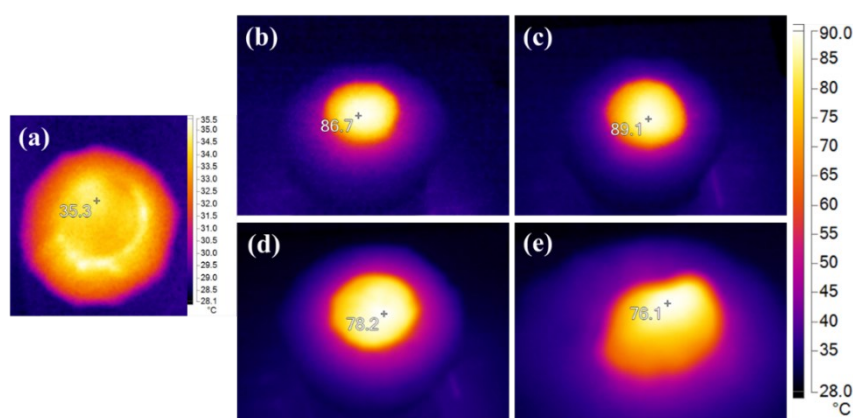


Figure S9 Temperature overlook of dry cryogels under one-sun irradiation for 20 min (a: PAAc, b: PAAc-PPy, c: PAAc-PANI, d: PAAc-GO, e: PAAc-rGO).

Determination of photothermal evaporation efficiency

Ignoring heat loss of evaporation system and considering the variation of evaporation enthalpy (ΔH_{evap}) only with temperature, the evaporation efficiency was calculated. However, abnormal results appear for the cases of PAAc-PPy and PAAc-GO sheets, suggesting that ΔH_{evap} should depend on cryogel structures.

Table S3 Summary of photothermal evaporation parameters under one-sun irradiation for 60 min.

cryogel sheet	η_{abs} (%)	R_{evap} ($\text{kg}\cdot\text{m}^{-2}\cdot\text{h}^{-1}$)	R_{real} ($\text{kg}\cdot\text{m}^{-2}\cdot\text{h}^{-1}$)	Q_{evap}^a (kJ)	Q_{heat}^b (kJ)	η_{evap} (%)	η_{total} (%)
PAAc-PPy	97.49	1.819	1.469	3525.6	100.1	103.30	100.71
PAAc-PANI	96.28	1.678	1.328	3187.2	92.7	94.63	91.11
PAAc-GO	66.94	1.551	1.201	2882.4	82.83	123.05	82.37
PAAc-rGO	85.47	1.585	1.235	2964	81.56	98.98	84.60

a: Heat for water evaporation within 60 min (Q_{evap}) was calculated with $\Delta H_{evap} = 2400 \text{ J}\cdot\text{g}^{-1}$ (40 °C).

b: Heat for heating water from room temperature (25 °C) to sheet surface temperature (T_{ave}). $C_{water} = 4.18 \text{ J}\cdot\text{g}^{-1}\cdot\text{K}^{-1}$ and $I_{inc} = 1 \text{ kW}\cdot\text{m}^{-2}$.

Comparison between current work and other reports

Table S4 offers the previous literature on the photothermal evaporation system, suggesting that our photothermal systems based PAAc cryogel have equivalent evaporation rate.

Table S4 Photothermal evaporation performance comparison between the current work and other reports (pure water under one-sun irradiation).

photothermal material	substrate material	evaporation rate ($\text{kg}\cdot\text{m}^{-2}\cdot\text{h}^{-1}$)	conversion efficient	Refs
Fe_3Si	melamine foam	2.08	91.8 %	10
GO and CNT	self-formed aerogel	1.62	83 %	11
GO film	PSt foam covered by cellulose	1.45	80 %	12
Ti_3C_2	paulownia wood	1.46	96 %	13
CuS	macroporous PAM hydrogel	1.46	92 %	14
carbon sponge	none	1.39	90 %	15
CNT	wood	0.95	65 %	16
	silica-gel	1.32	82 %	17
	cotton fabric	1.59	89.6%	18
core-shell Te-Se nanomaterial	PDDA-MS sponge	1.32	86.1 %	19
active carbon	PVA hydrogel	2.60	91 %	20
PPy	PVA cryogel ^a	3.2	94 %	21
	wood	1.01	72.5 %	22
	PI membrane	1.43	86.9 %	23

Abbreviations: PSt – polystyrene, PDDA – poly(diallyldimethylammonium chloride), MS – melamine sponge, PVA – poly(vinyl alcohol), PI – polyamide.

a: The hierarchically nanostructured gels (HNG) were frozen by liquid nitrogen and then thawed in deionized water at 30 °C. The freeze-thaw process was repeated ten times. Finally, the obtained HNG samples were freeze dried.

Photothermal evaporation with PAAc-PPy cryogel sheet with PAAc hydrogel substrate

Because of poor water transport inside PAAc hydrogel, the irradiations under four-sun for 60 min and under one-sun for 240 min lead the dehydration and warping of PAAc-PPy cryogel sheet as shown in Figure S10.

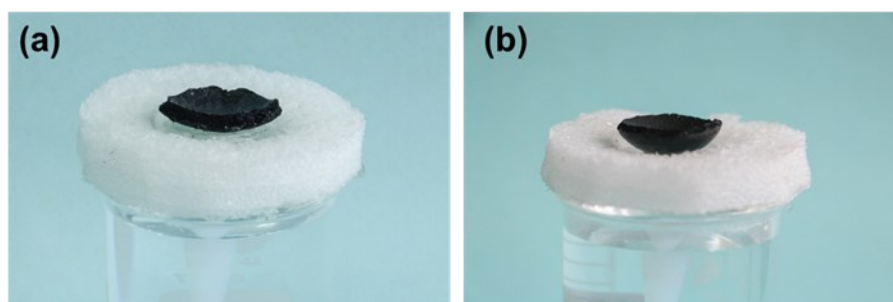


Figure S10 Photograph of PAAc-PPy cryogel sheet with PAAc hydrogel as the substrate (a: under four-sun irradiation for 60 min; b: under one-sun irradiation for 240 min).

During the photothermal evaporation under four-sun for 60 min, the surface temperature of composite cryogel sheet at the end and evaporation rate during steady evaporation are summarized in Table S5.

Table S5 The average and maximum temperatures of composite cryogel sheet at the top of PAAc cryogel or hydrogel substrate under four-sun irradiation for 60 min.

Cryogel sheet@substrate	T_{ave} (°C)	T_{max} (°C)	steady R_{evap} (kg·m ⁻² ·h ⁻¹)
PAAc@cryogel	48.0	50.1	2.249
PAAc-PPy@cryogel	57.0	60.1	6.492
PAAc-PPy@hydrogel	150.0	174.7	4.871 within 20-40 min 2.962 within 40-60 min
PAAc-PANI@cryogel	56.0	60.6	5.663
PAAc-GO@cryogel	56.4	61.5	5.407
PAAc-rGO@cryogel	58.5	62.7	5.652

During the photothermal evaporation under one-sun for 240 min, the surface temperature of composite cryogel sheet increases obviously and evaporation rate decrease noticeably within the late duration as shown in Figure S11.

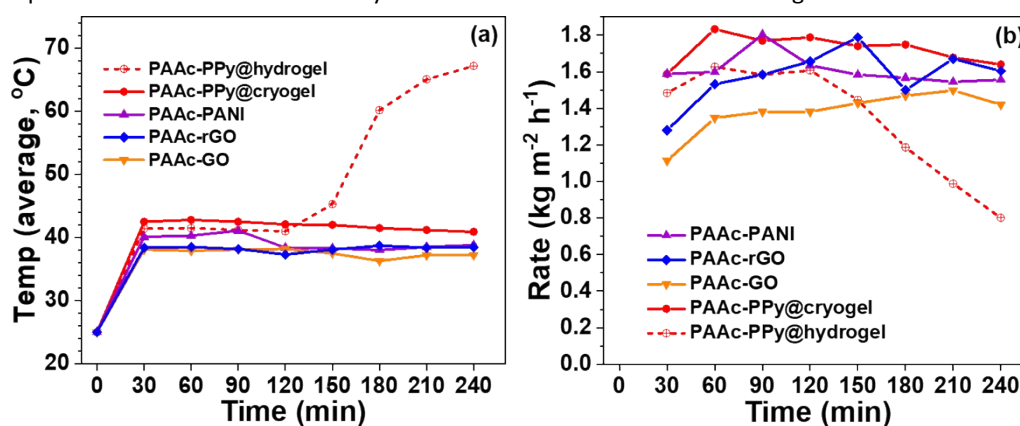


Figure S11 (a) Average temperature of cryogel sheet surface at different time, (b) Evaporation rate of pure water with cryogel/hydrogel substrate (one-sun irradiation for 240 min).

Reference

- Marcano D C , K D V , Berlin J M , et al., *Acs Nano*, 4 (8) (2010) 4806.
- Stankovich, S, Dikin, D A, Piner, R D, Kohlhaas, K A, Kleinhammes, A, Jia, Y, et al., *Carbon*, 45 (7) (2007) 1558-1565.
- Kaith, B S, Sharma, R, Kalia, S, *Int J Biol Macromol*, 75 (2015) 266-75.
- Veá-Barragan, A C, Bucio, E, Quintanar-Guerrero, D, Zambrano-Zaragoza, M L, Meléndez-López, S G, Serrano-Medina, A, et al., *Radiat Phys Chem*, 164 (2019).
- Chatterjee, A, Maity, S, *Surf Coat Tech*, 324 (2017) 569-576.
- Sara A S , U B, Mustafaev M I , et al. , *J Polym Sci Pol Chem*, 33 (10) (1995) 1581-1587.
- Rascón-Leon, S, Castillo-Ortega, M M, Santos-Sauceda, I, Munive, G T, Rodríguez-Felix, D E, Del Castillo-Castro, T, et al., *Polym Bull*, 75 (7) (2017) 3241-3265.
- Santos Saucedá, I, Castillo Ortega, M M, Tiburcio Munive, G, Quiroz Castillo, J M, del Castillo Castro, T, Encinas Romero, M A, et al., *Mater Chem Phys*, 182 (2016) 39-48.
- Yi, M, Shen, Z, Zhang, X, Ma, S, *J Phys D: Appl Phys*, 46 (2) (2013).
- Zhang, F, Li, Y, Bai, X, Wang, S, Liang, B, Fu, G, et al., *J Mater Chem A*, 6 (46) (2018) 23263-23269.
- Hu, X, Xu, W, Zhou, L, Tan, Y, Wang, Y, Zhu, S, et al., *Adv Mater*, 29 (5) (2017).
- Li, X, Xu, W, Tang, M, Zhou, L, Zhu, B, Zhu, S, et al., *Proc Natl Acad Sci U S A*, 113 (49) (2016) 13953-13958.
- Ma, N, Fu, Q, Hong, Y, Hao, X, Wang, X, Ju, J, et al., *ACS. Appl Mater Inter*, 12 (15) (2020) 18165-18173.
- Sun, Y, Gao, J, Liu, Y, Kang, H, Xie, M, Wu, F, et al., *Chem Eng Sci*, 207 (2019) 516-526.
- Zhu, L, Gao, M, Peh, C K N, Wang, X, Ho, G W, *Adv. Energy Mater*, 8 (16) (2018) 1702149.
- Chen, C, Li, Y, Song, J, Yang, Z, Kuang, Y, Hitz, E, et al., *Adv Mater*, 29 (30) (2017).
- Wang, Y, Zhang, L, Wang, P, *ACS. Sustain Chem Eng*, 4 (3) (2016) 1223-1230.
- Kou, H, Liu, Z, Zhu, B, Macharia, D K, Ahmed, S, Wu, B, et al., *Desalination*, 462 (2019) 29-38.
- Xing, C, Huang, D, Chen, S, Huang, Q, Zhou, C, Peng, Z, et al., *Adv Sci (Weinh)*, 6 (19) (2019) 1900531.
- Guo, Y, Zhao, F, Zhou, X, Chen, Z, Yu, G, *Nano Lett*, 19 (4) (2019) 2530-2536.

- 21 Zhao, F, Zhou, X, Shi, Y, Qian, X, Alexander, M, Zhao, X, et al., *Nat Nanotechnol*, 13 (6) (2018) 489-495.
- 22 Wang, Z, Yan, Y, Shen, X, Jin, C, Sun, Q, Li, H, *J Mater Chem A*, 7 (36) (2019) 20706-20712.
- 23 Xu, Y, Xu, H, Zhu, Z, Hou, H, Zuo, J, Cui, F, et al., *J Mater Chem A*, 7 (39) (2019) 22296-22306.

^a Address here.

^b Address here.

^c Address here.

† Footnotes relating to the title and/or authors should appear here.

Electronic Supplementary Information (ESI) available: [details of any supplementary information available should be included here]. See DOI: 10.1039/x0xx00000x